# A Hand-Activated White-Light Profilometry System to Effect the Automatic Recovery of Facial Shape

Padraig Butler[1], David Vernon[1] and Eoin O'Broin[2]

[1]Department of Computer Science, NUI Maynooth, Co. Kildare, Ireland.
E-mail: (pabutler, dvernon)@cs.may.ie

[2]Temple Street Children's Hospital,
Temple Street,
Dublin, Ireland.
E-mail: jack@indigo.ie

**Abstract.** In this paper, we present a face profiling system which incorporates two white-light stripe sources and a camera arranged in a dual triangulation configuration. The system overcomes many of the shortcomings associated with conventional laser profiling and CAT based systems. White light for example, emits significantly small levels of electromagnetic radiation to pose little threat to the skin and eyes. Two such light sources allow the complete recovery of facial surface information as the main occluded areas in one profile sequence are complementary to those in the other. The reflectance function of each light source approximates an intensity discontinuity whose position can be localised to a high degree of accuracy. An added advantage of white light is that the texture associated with each profile point may be recorded thus allowing a texture image of the scanned subject to be generated. This is of great benefit in applications where the aesthetic appearance of the face is of importance such as in this system's intended application - analysis of facial shape in the pre- and post- operative phases of reconstructive surgery. The optical system is mounted on an arm which is rotated about the subject by hand. Hand-actuation allows bulky motorised fixtures to be dispensed with and thus contributes largely to the portability of the system. However, the angular positions of the resulting non-uniformly sampled profiles must be computed. To facilitate this, a small angle encoder is used whose display is visible to the camera. The angles are computed from each image by visual recognition of the encoder display. A cylindrical elevation image and texture image is computed for each of the two profile sequences present in a scan. The data is then transformed to a Cartesian frame for rendering. Regarding current research, we present preliminary information regarding the means by which the two surfaces may be registered and combined so that a complete surface may be generated without occlusion. Also we present some current advances in the development of analysis software which effects the quantitative assessment of the regions of the facial surface that are of surgical relevance.

**Keywords:** white-light, texture, template matching, occlusion, encoder, calibration, cylindrical, Cartesian, registration.

## 1. Introduction

Reconstructive surgery addresses extremely difficult 3-D deformities in facial patients. Prediction and post-operative assessment of surgery in young patients with congenital defects over long periods of time involves accounting for cranial and tissue growth. To facilitate this, the surgeon must acquire geometric information which can sufficiently describe the morphology of the defect and allow the treatment to be determined. Traditionally this anthropometric information is determined manually using callipers and cephalostats. Such instruments yield little more than linear point to point measurements and are limited in accuracy. Computerised Axial Tomography (CAT) scan technology has been developed to allow 2-D transaxial slices of the body or head to be imaged using X-ray technology. CAT and MRI based measurements are very accurate but fail to provide valuable complex measurements such as facial tissue volume and surface area. In order to accommodate such measurements it is necessary to generate a 3-D surface model of the facial surface. This surface model may be characterised by a set of 3-D co-ordinates which together represent a large subset of the surface of the face.

Since the early 80's CAT software has been extended to allow a 3-D projection to be produced from a series of uniformly sampled 2-D slices[1, 2]. However, the expense and potential radiation hazard involved has inhibited the popularisation of such systems in the recovery of facial surface shape alone. Less hazardous structured light[3] and light striping[4, 5] systems however, have been routinely employed for the past decade. However, such systems fail to lend themselves for use in remote clinical trials due to their lack of portability. In this paper, we present a system which addresses the important issues of safety, portability, data accuracy and data completeness involved in the development of a light striping technique to effect the faithful recovery of a 3-D model of the face.

## 2. System Configuration

The physical scanning system incorporates a colour CCD camera centred between two white-light sources to form a dual triangulation configuration, Figure 1(a). The reflectance function of each light beam represents a vertically continuous series of intensity discontinuities, manifested as a high contrast narrow bar of light on the face. The camera is rotated by 90 degrees in order to maximise the number of samples that can be recorded along each imaged light stripe. The optical system is mounted on an arm which is free to rotate about a fixed axis. The line of intersection of the two light beams coincides with the principle axis of the camera at the axis of rotation. The subject to be scanned is positioned such that his/her head is centred beneath the axis in the field of view of the camera, Figure 1(b). The scanner is rotated about the

subject by hand thus allowing multiple left and right surface profile pairs to be imaged. Hand-actuation gives rise to non-uniformly sampled data. The circumferent position associated with each image is provided by an angle encoder whose display is fixed to the rotating arm in view of the camera. This allows the positional information associated with a sequence of light stripes to be encoded in the image information itself. The physical set-up incorporates a black velvet curtain as a backdrop to the scene. This eliminates the interference of extraneous background specular reflections in the subsequent processing of the image data. The image sequences are acquired using a PC based frame grabber and stored on CD to be processed off-line. The software for the system has been developed on a Sparc 20 using Khoros 2.1 and currently executes on a Sparc Ultra 2. An earlier version of the system is described in [6]. The current configuration differs from this mainly in that firstly, it incorporates a second light source, the justification of which is discussed in the next section. Secondly the registration target originally used to compute the rotation angle has been replaced by an encoder and display.

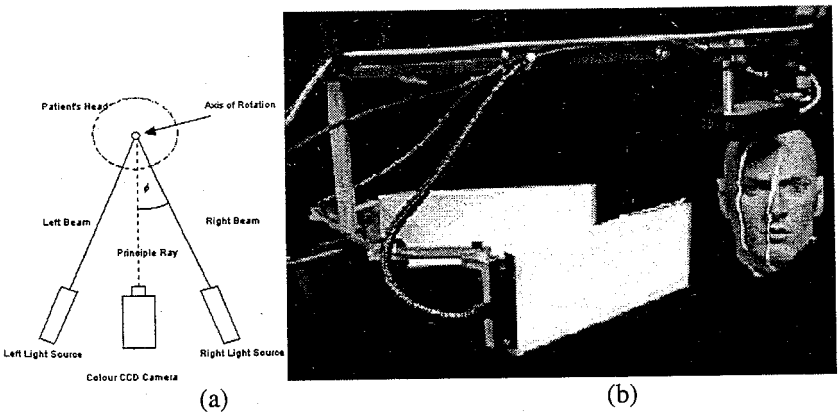


**Fig. 1.** (a) Schematic of configuration viewed from above. (b) Photograph of scanner.

## 3. Occlusion

To facilitate adequate depth recovery, the base-line separating the light source and camera must be sufficiently large. If it is two small, only significant variations in the morphology of the surface will be registered in the discrete image domain. Therefore the range of heights computable from each image will be greatly diminished, resulting in poor depth recovery.

However, regardless of the size of the base-line, a consistent problem exists. At certain positions about the face the reflected light becomes occluded by protruding features, particularly the nose, causing the associated imaged profile to be incomplete, Figure 2. This results in a loss of structural information about one side of the nose.

Reducing the base-line can minimise this problem. However, unless the base-line is zero the problem will almost always be present. Also, as mentioned earlier, reduction of the base-line increases the error associated with depth recovery. The occlusion problem can therefore only be solved by introducing a second light source and positioning it on the opposite side of the camera. Thus, each of the images constituting a scan sequence will contain a left profile and a right profile. The occluded region associated with the left profile sequence will complement that associated with the right. The two profile sets will together represent a complete surface.

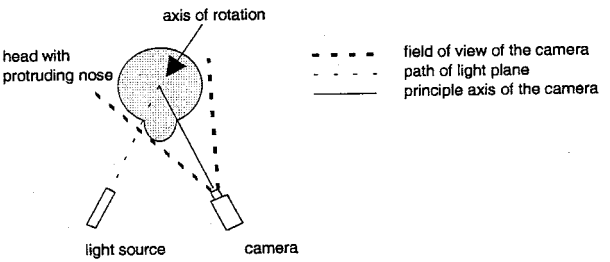


Light stripe is occluded by the nose and thus invisible to the camera.

**Fig. 2.** Schematic showing the occlusion effect.

## 4. Processing Prerequisites

The scan sequence comprises images which are acquired with the camera on its side. Therefore the sequence must be initially rotated by 90 degrees. Each rotated RGB image is divided into 2 sections, Figure 3. The two resulting sequences are processed independently.

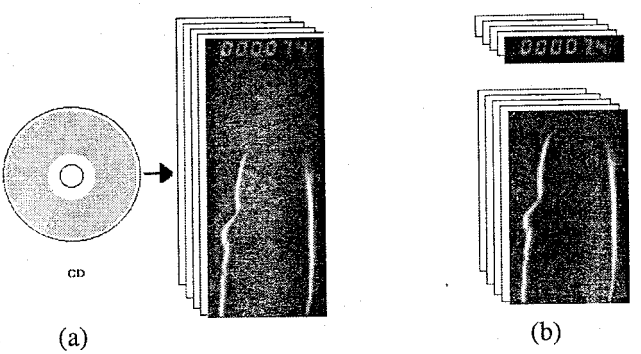


**Fig. 3.** (a) Sequence is read from off-line storage device and (b) divided into two sections.

The incoming image sequence is acquired in RGB format to accommodate the option of creating a colour texture image of the scanned subject. However the image processing software developed requires that the input sequence be represented in grey-scale. It is thus necessary to convert the RGB format to grey-scale by computing the intensity associated with each RGB triple comprising the readout sequence and the profile sequence. To accomplish this each sequence is converted from RGB to YIQ[7] using the transformation equation (1).

$$\begin{bmatrix} Y \\ I \\ Q \end{bmatrix} = \begin{bmatrix} 0.299 & 0.587 & 0.114 \\ 0.596 & -0.275 & -0.321 \\ 0.212 & -0.528 & 0.311 \end{bmatrix} \begin{bmatrix} R \\ G \\ B \end{bmatrix} \quad (1)$$

The Y value of the computed triple represents the luminance or intensity associated with the RGB value. The I and Q values represent chromaticity. The generation of the texture image using the retained RGB profile sequence will be described later.

## 5. Angle Computation

The position associated with each profile is given by the encoder readout. The display is visible to the camera and thus allows the position of each profile to be encoded visually in the image sequence. This eliminates the necessity for synchronisation between the encoder, camera and frame grabber. In order to compute the number present on each imaged readout, it is necessary to first compute the position of each of the 7 segment displays present. Since the readout is horizontally aligned with the top of the image, the vertical bounds of every digit present is constant. The digits comprising the readout are equally spaced and are of constant dimensions. If the position and dimension associated with each digit are known a set of 10 digit templates can be generated (representing the digits 0 - 9). If each template in turn is correlated with a digit sub-image, the template yielding the highest correlation will be deemed the most likely digit present at that position.

### 5.1 Computing Display Bounds

In order to compute the vertical and horizontal bounds of the encoder digits a calibration image must be generated in which all outer segments of each digit display are present. On occasion the first readout image in the sequence is sufficient as it usually comprises all zeros. However, in situations where this is not the case, the calibration image is generated by OR'ing all of the images of the readout sequence together.

A 1-D signature is computed which shows the position of the readout on the basis of its intensity. Each element of the signature is computed as the sum of all intensity values along its corresponding row in the calibration image. This is referred to as the horizontal projection of the image, Figure 4(a). The horizontal projection is thresholded to produce a simple binary pulse. The positions of the rising and falling edges of this pulse correspond to the vertical bounds of the display. The difference of these two values corresponds to the height ($h_{digit}$) of every digit comprising the readout.

Similarly, the horizontal bounds of each digit are computed from the vertical projection, Figure 4(b). The vertical projection is computed by summing each column of the calibration image. This projection is thresholded to produce a series of binary pulses. The positions of the rising and falling edges of these pulses correspond the horizontal start and end positions of the 7 segment displays present. The difference between each start and end pair should be approximately the same and should correspond to the width of a single digit ($w_{digit}$).

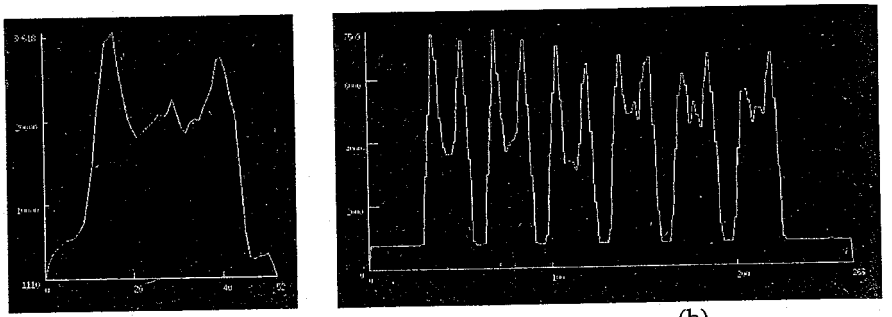

(a) (b)

**Fig. 4.** (a) Horizontal projection of readout image. (b) Vertical projection of readout image.

### 5.2 Template Generation

Each template is rectangular and has height equal to $h_{digit}$ and width equal to $w_{digit}$. In order to generate a template of each possible digit, it is necessary to take into account the physical appearance of each digit. In this case the outer segments form a parallelogram which leans slightly to the right. The width $w_{digit}$ of the template corresponds to the horizontal distance between the protruding corners of the digit. In order to generate a digit within the bounds of this template it is necessary to compute a digit's tilt angle. Since all segments comprising a digit are equal in length this angle may be computed simply from the diagram of Figure 5.

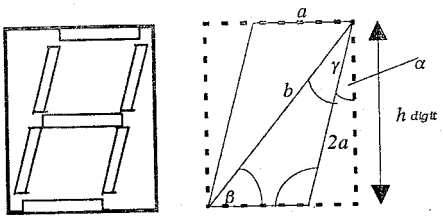


**Fig. 5.** Schematic representing digit dimensions within a template.

Distance $a$ represents the length of a single segment. Distance $b$ is the length of the major diagonal of the 7 segment display and is computed from equation (2). Angle $\alpha$ is the tilt angle and is computed from equation (6).

$$b = \sqrt{w_{digit}^2 + h_{digit}^2} \tag{2}$$

$$\beta = \tan^{-1}\left(\frac{h_{digit}}{w_{digit}}\right) \tag{3}$$

$$\frac{a}{\sin\gamma} = \frac{2a}{\sin\beta} \tag{4}$$

$$\Rightarrow \gamma = \sin^{-1}\left(\frac{\sin\beta}{2}\right) \tag{5}$$

$$\alpha = 90 - (\gamma + \beta) \tag{6}$$

$$t = \tan(\alpha) \tag{7}$$

Using the tilt gradient $t$ (equation (7)) it is now possible to generate segments of the appropriate length at appropriate positions within the template. The diagonal sides of the digit are generated by moving in a number of positions based on the tilt gradient before placing a white pixel representing a part of a segment which is on. Each digit from 0 to 9 is generated in this way. A lookup table is used to determine the segments to include when forming each digit template, Figure 6.

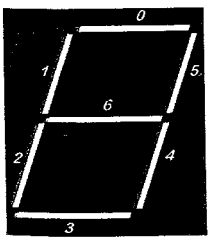


(a)

| | Seg 0 | seg 1 | seg 2 | seg 3 | seg 4 | seg 5 | seg 6 |
|---|---|---|---|---|---|---|---|
| 0 | on | on | on | on | on | on | |
| 1 | | | | | on | on | |
| 2 | on | | on | on | | on | |
| 3 | on | | | on | on | on | on |
| 4 | | on | | | on | on | on |
| 5 | | on | | on | on | | on |
| 6 | on | on | on | on | on | | on |
| 7 | on | | | | on | on | |
| 8 | on | on | on | on | on | on | on |
| 9 | on | | on | on | on | on | on |

(b)

**Fig. 6.** (a) Segment numbering convention. (b) Lookup table indicating segment representation for each digit.

**Fig. 7.** Typical set of digit templates.

Normalised cross correlation is carried out between the digit sub-image and the white regions of the template since it is these regions that constitute the relevant segment information. A typical set of templates is shown in Figure 7. The template yielding the maximum correlation with an image sub-section is deemed the most likely digit to be present. This procedure is carried for all display positions and the angle is computed.

### 5.3 Synchronisation Issues

The encoder used has a 6 digit display and can register the angular position of the scanner's arm to 0.1 of a degree accuracy. One problem that this introduces is that when rotating about an object to achieve approximately 130 degree coverage in 4 seconds, the lack of compatibility between the encoder display and the imaging system becomes apparent. The imaging system acquires images at 25 frames per second.

Due to the frequency of the $10^{th}$ of a degree digit changing and the default shutter speed of the camera being 1/25 seconds, approximately 13 new values occur per frame. This means that in each image of the sequence, the digit behind the decimal point will almost always appear ambiguous and the first digit before the decimal point will quite frequently appear ambiguous. This is because the 13 digits are effectively averaged during the sensor's integration period. As mentioned, the default integration time on the CCD camera is 1/25 seconds. In a typical scan the encoder display updates every 1/325 seconds. In order to reduce the occurrence of ambiguous digits, it is thus necessary to decrease the integration time for the camera. The next two settings on the camera are 1/60 seconds and 1/125 seconds. Going beyond 1/125 seconds greatly diminishes the image quality even when the gain is manually increased. Also, since the set of seven segment displays on the encoder are multiplexed this feature becomes visible when the shutter speed is increased any further.

In order to minimise the effects of this speed incompatibility the encoder circuitry has been modified so that the display will only update every 0.4 degrees. This means that in a typical scan the encoder will update only 80 times per second. This modification combined with the increased shutter speed of 1/125 seconds allows only 1 update approximately, to occur per frame leaving the likelihood of ambiguous digits appearing in a sequence minimal. However since the camera and encoder display are not synchronised, it is still possible for some angles to be incorrectly

recognised. Figure 8(a) shows a plot of a typical set of angles computed from a scan sequence comprising 100 images.

Since the rotation is smooth, the angles form a curve. The two peaks present in the plot represent angles which are out of sequence with the rest. Each of these angles comprise digits which cannot be correctly recognised due to their ambiguous appearance. In order to estimate the values that these angles should represent, the data is filtered. When a value interferes with the continuity of the curve, it is replaced by the average of its two neighbouring values. Figure 8(b) shows the same data set with the incorrect angles removed. Note that the only data values that have been changed are those corresponding to the peaks in Figure 8(a).

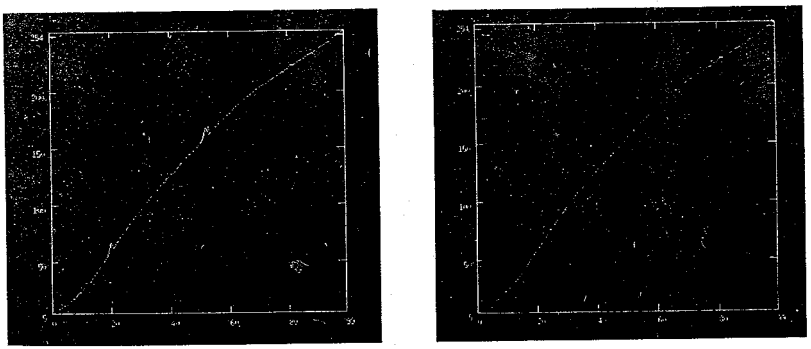

(a) (b)

**Fig. 8.** (a) Graph representing a set of computed angles, peaks indicate incorrectly recognised angles. (b) Conditional mean filtering to remove incorrect angles.

In order to allow for the possibility of inter-frame angle changes, a polynomial of order 8 is fitted the final set of computed angles. This allows the fine transitions from angle to angle to be approximated on the basis that the rotation of the optical system is smooth and should represent a curve. The polynomial is generated using the method of least squares[8]. An over determined system of equations is generated using the input 2-D points (i.e. image number and angle). The equations represent polynomials of pre-defined but equal order where the coefficients are the unknowns. For any chosen order, the coefficients associated with a polynomial which most closely resembles the function represented by the input set of $(x, y)$ points will be computed.

# 6. Profile Localisation

We define a profile as a series of points connected vertically which together describe the point to point height variation along the surface of the face at any one position. As mentioned in section 2, the scanner configuration utilises white light whose reflectance function approximates an intensity discontinuity. This introduces a significant advantage in that the reflected stimulus to be measured is an inherent point like entity. Thus, a series of vertically connected points defining the shape of the face at a single position is encoded in the imaged light stripe. In order to make this profile information explicit it is necessary to identify the position where the dark to light intensity discontinuity occurs for each and every position along the length of the imaged light stripe. The algorithm used to accomplish this yields repeatability accuracy of less than 0.1 pixels and is described in [6, 9].

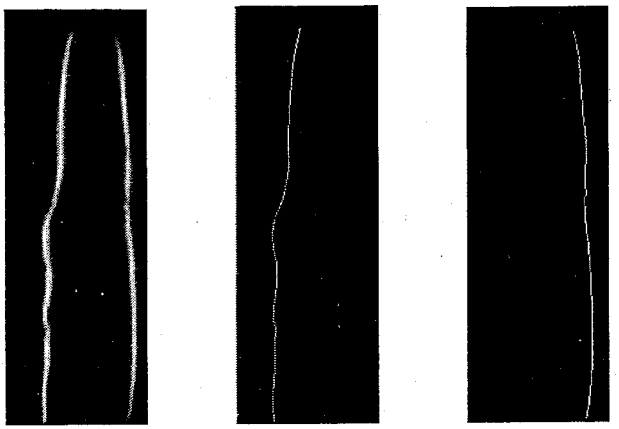


**Fig. 9.** (a) Raw profile pair. (b) Segmented left profile. (c) Segmented right profile.

Each image of the profile intensity sequence is processed in two halves, see Figure 9. The edge of each of the left profiles is computed by applying the localisation algorithm to the left side of each image, Figure 9(b), and vice versa for the right, see Figure 9(c). The resulting edge profiles are stored in two separate sequences. The sub-pixel position of each edge is encoded as a floating point grey-level and stored in the nearest pixel.

## 6.1 Texture Recovery

One of the significant advantages of using white light pertains to texture recovery. Using the edge information associated with a single image, the corresponding RGB texture information may be deduced from the original RGB image. The edge is however, likely to occur somewhere between the dark and bright region of the step

discontinuity, so its intensity may not be sufficient to represent brightly enough, the texture associated with the edge point. It is because of this that the approximate texture corresponding to the point is taken 2 to 3 pixels to the right of the edge position. Since the edge position is almost always non-integer the position of the corresponding texture value will also be non-integer. The appropriate texture is thus estimated by linear interpolation over the RGB values to the left and right of this position. This allows the creation of a set of RGB colour profiles matching in structural appearance, the set of edge profiles. This provides the raw material for producing a texture image of the face.

### 6.2 Safety

Another advantage associated with the use of white light in an application of this kind pertains to eye and skin safety [10]. If a person is exposed to laser radiation, eye safety is an important issue. Some lasers emit hazardously high levels of electromagnetic radiation. This may be in the form of visible or invisible light. The human eye is very sensitive to such radiation and exposure to this may result in long term damage to the cornea or retina. The area of damage is dependent mainly on the wavelength of the light and the duration of exposure. White light emits significantly smaller levels electromagnetic radiation and thus poses less of a threat to the human eye and skin.

## 7. Profile Height Computation

The deviation of each point along a single localised profile is computed as the perpendicular distance from that point to the vertical line corresponding to the axis of rotation of the scanner. This deflection value is proportional to the radial height of the corresponding real surface point with respect to the same axis. The relationship can be computed from Figure 10 to give equation (8).

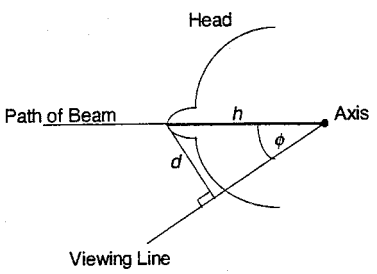


**Fig. 10.** Orthographic relationship between radial height and beam deflection.

$$h = \frac{d}{\sin\phi} \tag{8}$$

This, however, represents an orthographic projection and doesn't take into account the perspective distortion incurred on the imaged point as a result of the projection process. The correct relationship is computed from Figure 11 to give equation (9). The parameters $u$, $f$, $\phi$ are constant and thus the relationship may be rewritten to give equation (10).

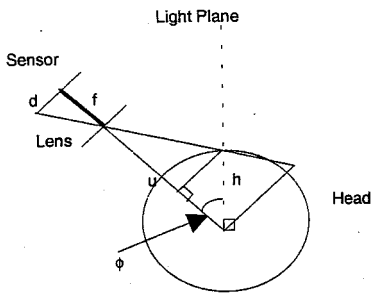


$u$ = distance from centre of lens to axis
$f$ = focal length of lens
$\phi$ = angle between light source and camera
$d$ = deflection of profile point on sensor
$h$ = radial height of profile point corresponding to $d$

**Fig. 11.** Perspective relationship between beam deflection and radial height.

$$h = \frac{d(u-f)}{\left(f\sin\phi + d\cos\phi\right)} \tag{9}$$

$$h_i = \frac{d_i k_1}{\left(k_2 + d_i k_3\right)} \tag{10}$$

In order to model this projection it is necessary to compute the values associated with unknowns $k_1$, $k_2$, $k_3$. Rewriting equation (10) reduces the number of unknowns to 2 giving the linear equation (11).

$$h_i a + h_i d_i b = d_i \text{ where } a = \frac{k_2}{k_1}, b = \frac{k_3}{k_1} \tag{11}$$

To find a solution for $a$ and $b$, at least 2 profile deflection values must be provided along with their corresponding real height values. For the purpose of this work, 8 height, deflection pairs are used to over determine the system of linear equations and the coefficients $a$ and $b$ are solved using the method of least squares.

The height, deflection pairs are acquired with the aid of a calibration object. The calibration object consists of a black plane inclined at 45 degrees. Equally spaced white points are marked along the incline. The object is positioned such that the first of these points coincides with the axis of rotation and corresponds to a radial height of 0 *mm*. All subsequent points extend outwards towards the camera representing

points of equally varying height. The optical system is rotated until one of the vertical light beams intersects all of these points. The object is then imaged to produce a series of points whose positions are localised using the profile edge localisation algorithm referred to in section 6. The deflections are then computed with respect to the position of the first point which corresponds to the axis of rotation. Each deflection value is associated with a known real-world height measured from the calibration object. This calibration phase is performed for both light sources and two separate transformations are computed. Thus, the height associated with every point along the left and right imaged profiles can be computed.

The accuracy of profile height computation depends greatly on the accuracy to which the deflection of each profile point can be measured. Thus the accuracy of the calibration phase and the profile edge localisation is pertinent.

## 8. Profile Accumulation and Surface Estimation

The computed elevation profiles represent the surface morphology of the face sampled in a cylindrical manner. In order to generate a complete profile description of the face these profiles must be accumulated into a single frame. The position of each profile is dictated by the angle at which it was acquired. The profiles are accumulated into a single image where the angular position is represented along the horizontal axis and the elevation data is represented by intensity. Since the non-integer angle positions cannot be represented in the discrete image domain each pixel is given an associated real 3-D location which encodes the position of each profile point in an $x$, $y$, $z$ co-ordinate. The Khoros image data format accommodates for the storage of this extra information within an image, (location data[11]). A profile elevation image is generated for left and right profile sequences constituting a scan.

The associated texture profiles for each profile sequence are accumulated in the same manner. However, since it is only intended that these profiles represent the approximate texture associated with the elevation data, location data is not used and each profile is placed in the nearest integer position corresponding to its associated angle.

### 8.1 Estimating the Inter-Profile Information

The inter-profile information is computed using Lagrange's interpolation method. The interpolation is performed on each row of the two elevation profile images. The algorithm accommodates interpolation on either image data or location data. Each missing point is interpolated on the basis of its left and right neighbouring values. If the number of interpolation points chosen is 2 (1 left and 1 right), the interpolation is linear. For the purpose of this application 2 existing points to the left and right of each missing point has proven adequate for relatively smooth surface recovery.

As it is likely that regions of missing data corresponding to occlusion will be present in both profile images, it is necessary for the interpolation program to ignore these regions. Areas of occlusion are defined as those regions associated with breaks in profiles. A mask image is generated that consists of vertical lines placed at all positions corresponding to profile positions. The mask image represents all the regions among the profiles where data should be present initially. A region will not be interpolated if there is no data point in the profile image corresponding to a valid region of the mask image. Figure 12(a) shows an elevation image generated from a sequence of left profiles sampled from a mannequin's face. Figure 12(b) shows the elevation image associated with the right profile sequence of the same scan. Note that the regions of occlusion about the nose have not been interpolated.

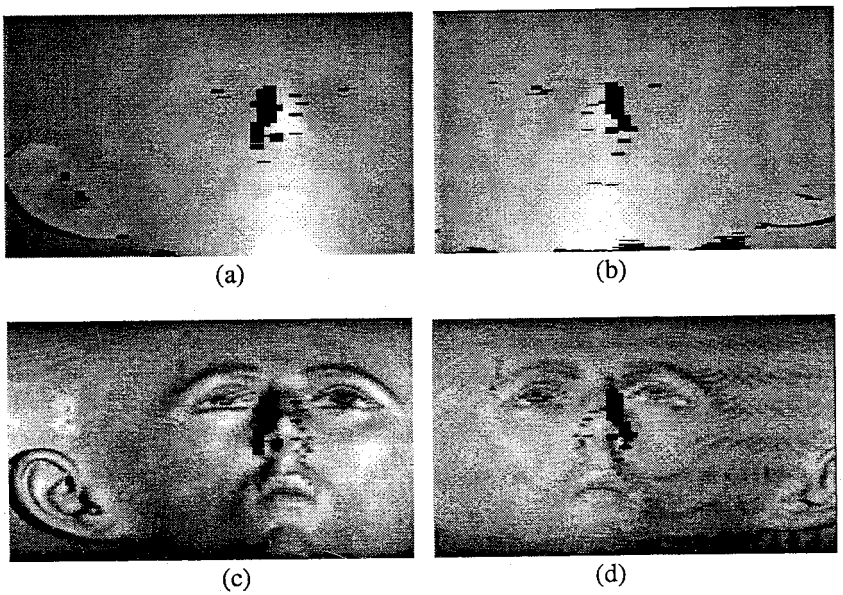


**Fig. 12.** (a) Elevation image computed from the left profile set. (b) Elevation image computed from the right profile set. (c) Texture image generated from the left profile set. (d) Texture image generated from the right profile set.

The inter-texture profile information is computed in the same way. However, linear interpolation has proven sufficient for this purpose. The interpolation is carried out on each band independently such that the gradual change in the R, G and B band intensities an be approximated. The result is a cylindrical surface texture image of the scanned subject. Two texture images are generated, one for the left profile sequence (Figure 12(c)) and one for the right profile sequence (Figure 12(d)).

### 8.2 Cartesian Representation

The appropriate representation of the elevation data is Cartesian. It is thus necessary to transform the existing cylindrical surface elevation image to its Cartesian equivalent. The transformation is applied to the location data section of each of the two elevation images. The original cylindrical data is maintained in the intensity segment of the image and the Cartesian equivalent is stored in the location segment. A quadrilateral mesh is fitted to the location data to facilitate visualisation of the surface using a Khoros rendering tool, Figure 13. It is not necessary to transform the texture data as each texture point is automatically associated with a cylindrical elevation point which is associated by image position with its Cartesian equivalent.

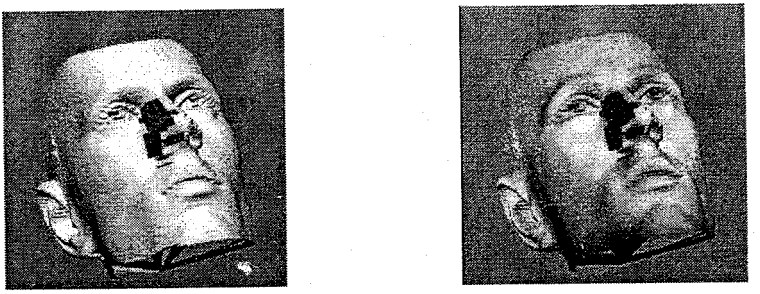

**Fig. 13.** (a) Rendered surface representing left profile set without overlaid texture. (b) Rendered surface with overlaid texture.

## 9. Current Research

### 9.1 Surface Registration

Having successfully generated two surfaces exhibiting opposite regions of occlusion, these surfaces must be registered so that they can be combined to produce a single complete surface. In light of this, software effecting the registration of two such surfaces is currently under development. The primary objective of the software is to register one surface with respect to the other until the similarity measure between the two is maximised. The registered image is computed as the transformation of one surface with respect to the other. All possible transformations, within some bounds, are tested. A coarse to fine strategy is employed in the search for the transformation which yields the best similarity measure. The difference measure is defined in terms of both the image data and the gradient of the first input image. Specifically the difference is defined as the RMS difference between the first image and the second

image. The output registered image is the second input image transformed by the translation, rotation and scaling which minimises the RMS difference between the two images. The registration is only performed on valid image data corresponding to the non-zero regions of both inputs. The registration software is not yet complete and so the information above cannot yet be substantiated with results.

### 9.2 Surface Combination

A pair of successfully registered images are combined through a conditional blend. This involves averaging the corresponding non-zero regions of two images. The regions of zero data in one image are replaced by corresponding regions of non-zero data present in the other. This allows the complementary non-occluded regions of two registered surface images to be combined, thus producing a complete surface. This software has been successfully tested on synthetic data including a set of similar 2-D Gaussians with different regions removed (thus mimicking occlusion) which when manipulated by the software produced the original single complete Gaussian. Testing may be completed when the registration software (see section 9.1) is completed.

### 9.3 Surface Analysis

Concerning analysis, some preliminary software effecting surface and linear measurements has been developed and is currently being tested. This software quite effectively facilitates the computation of manually inaccessible measurements in order to build a quantitative description of regions of surgical relevance. The software accommodates the computation of surface volume, surface area, area of projection, surface distance of the maximal chord and Euclidean distance of the maximal chord associated with any 2-D surface either representing an entire face or an interactively selected region of the face. Some preliminary clinical studies are presented in[12].

## 10. Conclusions

A profilometry system effecting the recovery of facial shape has been presented. The use of white-light accommodates optional texture recovery and contributes to the safety aspect of the system. Occlusion is dealt with by incorporating two light stripe sources to form a dual triangulation configuration. The imaged profile pairs constituting a scan can be are localised to a high degree of accuracy. The scanning process is hand activated, and thus contributes greatly to the portability of the system. The position of each profile pair is computed through character recognition of a 7 segment encoder display which is present in each image. Two elevation images and

two texture images are computed per scan. Surface registration and analysis procedures have been presented as work in progress. This software will allow quantitative assessment to be carried out on surface regions in the pre- and post-operative phases of reconstructive surgery.

## References

[1] Vannier M. W, Marsh J. L, Warren J. O, "Three Dimensional Computer Graphics for Craniofacial Surgical Planning and Evaluation", Computer Graphics, vol. 17, no. 3, July 1983, pp 263 - 273.

[2] Moss J. P, Linney A. D, Grindrod S.R, Arridge S. R, Clifton J. S, Three Dimensional Digitisation of the Face and Skull using Computerised Tomography and Laser Scanning Techniques", European Journal of Orthodontics 1987, vol. 9, pp 247 - 253.

[3] Commean P. K, Smith K. E, Bhatia G., Vannier M. W, "Geometric Design of a Multisensor Structured Light Range Digitiser", Optical Engineering, April 1994, vol. 33, no. 4, pp 1349 - 1358.

[4] Moss J. P, Linney A. D, Grindrod S. R, Mosse C. A, "A Laser Scanning System for the Measurement of Facial Surface Morphology", Optics and Lasers in Engineering, vol. 10, 1989, pp 179-190.

[5] Cutting C. B, Mc Carthy J. G, Kerron D. B, "Three Dimensional Input of Body Surface Data using Laser Light Scanner", Ann. Plast. Surg., 1988, vol. 21, no. 1, pp 38-45.

[6] Butler P, Vernon D, O'Broin E, "Estimation of a 3-D Surface Profile of the Human Face using a Hand-Actuated White-Light Profilometer", First Pan-Irish Conference on Machine Vision and Image Processing, Magee College, University of Ulster, (1997).

[7] Foley J, Van Dam A, et al, " Introduction to Computer Graphics", Addison Wesley, 1994, pp 410 - 419.

[8] Ballard D. H, Brown C. M, "Computer Vision", Prentice-Hall, Englewood Cliffs, New Jersey 07632, 1982, pp484 - 488

[9] Vernon D, Butler P, O'Broin E, "Edge Localisation in a White-Light Profilometer with Sub-Pixel Accuracy", Lasers in Optical Engineering '97, 2nd Annual Conference of the Optical Engineering Society of Ireland, Galway, Ireland (1997).

[10] Sanz J. L. C, "Advances in Machine Vision", Springer Verlag, NY, 1989.

[11] Khoral Research Inc., "Khoros Pro Users Guide", Khoral Research Inc, 6001 Indian School Rd, suite 200, Albuquerque, NM 87110, USA, August 1, 1996, ppI-47 - I-49.

[12] O'Broin E, Early M. J, Butler P, Vernon D, "A New 3-D Scanning System: A Preliminary Clinical Study", American Cleft Palate - Craniofacial Association, 55th annual meeting, Baltimore, 24th April, 1998.

| *Scene Number and Content* | 0° orientation sensor image | 90° orientation sensor image | Simple Average Reconstruction | Constrained Reconstruction |
|---|---|---|---|---|
| Scene 1: Child | 7.7 | 9.04 | 6.6 | 5.03 |
| Scene 2: Seagull | 19.27 | 13.59 | 13.09 | 9.8 |
| Scene 3: Nerve cell | 10.51 | 10.29 | 8.06 | 5.89 |
| Scene 4: Moonscape | 7.7 | 9.31 | 7.17 | 5.92 |
| Scene 5: VW Boot | 32.12 | 21.42 | 22.12 | 16.7 |

**Table 1.** Figure of merit values for each scene using the unstaggered sensor geometry. These figure-of-merit values are estimated by computing the root mean square (RMS) of the difference values (pixel errors) between the reconstructed image and the orginal image for five scenes.

| *Scene Number and Content* | 0° orientation sensor image | 90° orientation sensor image | Simple Average Reconstruction | Constrained Reconstruction |
|---|---|---|---|---|
| Scene 1: Child | 8.66 | 9.55 | 7.5 | 5.67 |
| Scene 2: Seagull | 20.04 | 15.98 | 15.11 | 11.49 |
| Scene 3: Nerve cell | 11.36 | 11.21 | 9.08 | 6.57 |
| Scene 4: Moonscape | 8.66 | 9.76 | 8.06 | 6.64 |
| Scene 5: VW Boot | 34.21 | 26.44 | 27.2 | 21.94 |

**Table 2.** Figure of merit values for each scene using the staggered sensor geometry. These figure-of-merit values are estimated by computing the root mean square (RMS) of the difference values (pixel errors) between the reconstructed image and the orginal image for five scenes.

David Vernon (Ed.)

# OESI–IMVIP '98

## Optical Engineering Society of Ireland & Irish Machine Vision and Image Processing Joint Conference

## PROCEEDINGS

National University of Ireland, Maynooth
9th-10th September, 1998

NUI MAYNOOTH
Ollscoil na hÉireann Má Nuad

Cumann Innealtóireacht Optúla

THE OPTICAL ENGINEERING SOCIETY OF IRELAND